Title: Perceptual cycles travel across retinotopic space

Abbreviated Title: Perceptual cycles travel

Author names and affiliations, including postal codes:

Camille Fakche[1] and Laura Dugué[1,2]

[1] Université Paris Cité, CNRS, Integrative Neuroscience and Cognition Center, F-75006 Paris, France

[2] Institut Universitaire de France (IUF), F-75005 Paris, France

Corresponding author email address:

camille.fakche@gmail.com

Number of pages: 33.

Number of figures: 5.

Number of tables, multimedia, and 3D models: 0.

Number of words abstract: 244.

Number of words introduction: 604.

Number of words discussion: 1500.

Conflict of interest statement: The authors declare no competing financial interests.

Acknowledgements: This project has received funding from the European Research Council (ERC) under the European Union's Horizon 2020 research and innovation program (grant agreement No 852139 – Laura Dugué) and the Agence Nationale de la Recherche (ANR) - Deutsche Forschungsgemeinschaft (DFG) program (grant agreement No J18P08ANR00 – Laura Dugué). We also thank Kirsten Petras, Andrea Alamia, Rufin VanRullen and Frédéric Chavane for their useful comments on the manuscript.

Abstract (244/250 words)

Visual perception waxes and wanes periodically as a function of the phase of low-frequency brain oscillations (theta, 4-7 Hz; alpha, 8-13 Hz). Perceptual cycles are defined as the corresponding periodic modulation of perceptual performance. Here, we tested the hypothesis that brain oscillations travel across the visual cortex, leading to predictable perceptual consequences across the visual field, i.e., perceptual cycles travel across the retinotopic visual space. An oscillating disk (inducer) was presented in the periphery of the visual field to induce brain oscillations at low frequencies (4, 6, 8 or 10 Hz) at a specific retinotopic cortical location. Target stimuli at threshold (50% detection) were displayed at random times during the periodic disk stimulation, at one of three possible distances from the disk. Electroencephalography (EEG) was recorded while participants performed a detection task. EEG analyses showed that the periodic stimulation produced a complex brain oscillation composed of the induced frequency and its first harmonic likely due to the overlap of the periodic response and the neural response to individual stimuli. This complex oscillation, which originated from a precise retinotopic position, modulated detection performance periodically at each target position and at each frequency. Critically, the optimal behavioral phase, i.e., of highest performance, of the 8 Hz and 10 Hz oscillations (alpha range) consistently shifted across target distance to the inducer. Together, the results demonstrate that alpha-induced perceptual cycles travel across the retinotopic space in human observers at a propagation speed ranging from 0.3 to 0.5 m/s.

Significance Statement (103/120 words)

Visual perception is modulated periodically as a function of the phase of theta-alpha brain oscillations in the occipital cortex, i.e., perceptual cycles. We hypothesized that brain oscillations travel across the visual cortex, which in turn would result in the propagation of perceptual cycles across the retinotopic visual space. Using psychophysics coupled with EEG recordings, our study showed that the phase of alpha brain oscillations associated with the highest visual performance consistently shifted across the visual space. Perceptual cycles

traveled across the retinotopic space in human. The propagation speed ranged from 0.3 to 0.5 m/s consistent with the conduction delay of long-range lateral connections.

Introduction (604/650 words)

Visual perception fluctuates rhythmically along with the phase of low-frequency brain oscillations (theta, 4-7 Hz; alpha, 8-13 Hz) (Valera et al., 1981; Busch et al., 2009; Mathewson et al., 2009; Dugué et al., 2011, 2015; Samaha and Postle, 2015, Samaha et al., 2017; Fakche et al., 2022; Merholz et al., 2022; for review: VanRullen, 2016; Kienitz et al., 2022; Keitel et al., 2022). Studies suggest that this phase effect accounts for less than 20% of the trial-by-trial variability in behavioral performance (Busch et al., 2009; Busch and VanRullen, 2010; Dugué et al., 2011, 2015; Baumgarten et al., 2015; Samaha et al., 2017; Fakche et al., 2022). We hypothesize that if brain oscillations are the support of visual perception, they should explain a larger portion of the variance observed in empirical data. We propose that not only the temporal aspect of brain signals but also their spatial organization must be jointly considered when investigating their functional role.

Invasive studies in mammals reveal that low-frequency oscillatory activity propagates within individual visual areas (V1, V2, V4, MT) with a phase shift between the source of the neural activity and more distal retinotopic positions (Sanchez-Vives and McCormick, 2000; Huang et al., 2004; Benucci et al., 2007; Han et al., 2008; Ray and Maunsell, 2011; Maris et al., 2013; Stroh et al., 2013; Muller et al., 2014; Townsend et al., 2015; Zanos et al., 2015; Davis et al., 2020). In humans, although a few invasive studies in patients showed that low-frequency oscillations can propagate within individual non-visual brain areas (Takahashi et al., 2011; Zhang and Jacobs, 2015; Sreekumar et al., 2021), there is no electro-physiological study to date investigating the propagation of low-frequency oscillations in individual visual areas. This may be due to several methodological constraints including, for invasive studies, the usual lack of intracranial coverage over the visual system, and for non-invasive studies, the poor spatial

resolution of magnetoencephalography (MEG) and EEG. The aim of the present study is to circumvent these issues.

Sokoliuk and VanRullen (2016) proposed that the propagation of visually-induced oscillations across the *cortical* retinotopic space influences perceptual performance across the *visual* retinotopic space. With a psychophysics experiment, they showed that the optimal phase, i.e., associated with the highest detection performance of a small, low-contrast target stimulus, shifted as a function of the distance from the visual inducer, suggesting that induced-oscillations at 5 Hz and 10 Hz were propagating across retinotopic space. Here, we used the same psychophysics approach. We additionally recorded EEG to identify the shape of the induced-oscillations, and eye-tracking to ensure successful fixation of the center of the screen, critical for stable retinotopic representation. Other critical changes were made to the design, including the size of the targets, which was adjusted to cortical magnification, so that each stimulus activated the same number of neurons in the cortical retinotopic space. Additionally, we parametrized the frequencies by testing four different frequencies in the theta/alpha range (4, 6, 8, and 10 Hz), which was done in each participant (n=17) to ensure robust statistical analyses (in Sokoliuk and VanRullen, n=5 for 5 Hz, n=7 for 10 Hz and n=15 for a 10-Hz replication set).

Our study assesses the propagation of low-frequency brain oscillations across the visual cortex, leading to the propagation of perceptual cycles across the retinotopic space. Contrary to the earlier study (Sokoliuk and VanRullen, 2016), our results demonstrate that alpha-induced perceptual cycles, and not theta, traveled across the retinotopic space in human observers at a propagation speed ranging from 0.3 to 0.5 m/s consistent with the conduction delay of long-range lateral connections (Shao and Burkhalter, 1996; Nowak and Bullier, 1996; Girard et al., 2001).

Materials and Methods

Participants

18 participants (9 females, 16 right-handed, mean ± sd age: 26.2 ± 4.1 years) were recruited for the experiment (based on Sokoliuk and VanRullen, 2016). One participant was excluded from the analysis because the number of false alarms exceeded the number of targets presented. 15 participants (7 females, 13 right-handed, mean ± sd age: 25.5 ± 3 years) were recruited for an additional control experiment. All participants were free from medication affecting the central nervous system, reported no history of psychiatric or neurological disorders, gave their written informed consent and were compensated for their participation. The study was approved by the local French ethics committee Ouest IV (IRB #2020-A00859-30) and followed the Declaration of Helsinki.

Stimuli

Stimuli were designed with PsychToolbox 3.0.12, running in Matlab R2014b 64-bit (The MathWorks, Natick, MA), and displayed with a ProPixx Projector (VPixx Technologies, Saint-Bruno, QC, Canada), on a 139 x 77.5 cm projection screen (1920 x 1080 pixels; 480 Hz refresh rate), at 122 cm distance. Three different stimuli were generated: a fixation cross, a peripheral disk, and three small dots (targets). The arms of the fixation cross measured 0.15 degrees of visual angle (°) of length and 0.03° of width. The size and position of the targets were computed according to cortical magnification (Human cortical magnification factor = $\frac{23.07}{eccentricity + 0.75}$ Horton and Hoyt, 1991) so that each target (diameter) represented a 0.8 mm portion of cortex spaced by 0.8 mm edge-to-edge (radius: 0.09°, 0.1° and 0.12°; eccentricity: 4.1°, 4.5° and 4.9°). The peripheral disk (inducer) was displayed on the lower right corner at 7.5° of eccentricity (from the center of the disk; radius: 1.75°). The background color was black, and the fixation cross at 50% of contrast relative to the background. Target contrasts were titrated for each participant, each position, and each frequency, using a staircase procedure (see below). The peripheral disk was oscillating sinusoidally in luminance, from black to white (i.e., from 0% to 100% of contrast; one period: black-to-white-to-black), at frequencies in the theta

and alpha range: 4.07, 6.13, 8.27 and 10.43 Hz. For clarity, we rounded these values to 4, 6, 8, and 10 Hz.

Eye tracker

Participant's head was maintained with a headrest and chinrest. An infrared video-camera system (EyeLink 1000 plus 5.08, SR Research, Ottawa, Canada) was used to ensure that participants maintained their gaze on the fixation cross throughout the block. The block only started when participants was successfully maintaining fixation. When a gaze deviation of >2° from the center of the screen was detected during the presentation of a target (-150 ms to +100 ms around target onset) or a blink, we considered that the participant broke fixation and the trial was removed from the analysis (129.1 ± 120.9 trials on average across participants, leading to a total number of trials of 5015.2 ± 199.9 trials per participant). Supernumerary blocks were added at the end of each run to compensate for rejected trials. Participants received feedback at the end of each block to remind them to minimize blinking and to maintain fixation.

EEG

EEG was recorded using a 64-channels actiChamp system (Brain Products GmbH). The ground was placed at the Fpz position, and the right mastoid was used as reference (DC recording; 1000 Hz sampling rate).

Experimental Design

Participants performed five sessions: four psychophysics sessions (one session for each induced frequency; frequency order randomized across participants), and one EEG session. The psychophysics sessions were composed of the staircases and two runs of 50 blocks each. The EEG session contained four runs of 24 blocks each (one run for each induced frequency).

For both the staircases and the main task, each block lasted 30 seconds during which the peripheral disk continuously oscillated in luminance. 6 to 18 targets were presented at random

times (excluding the first and the last seconds, and with at least one second interval between targets) during three frames (6.3 ms) according to a decreasing probability distribution (~10 targets per block on average). The number of targets for the three positions was randomized across blocks (and pseudorandomized across runs). Participants were instructed to press the space bar when they detected a target (in a 1-second time window after which their response was not considered; target presentation and response window composed a trial).

A one-up/one-down staircase with decreasing steps was performed separately for each target position to titrate the contrast of the target to reach about 50% detection. Each staircase was composed of 7 blocks, as described above, except that the targets appeared always at the same position. During the main task, target contrasts were adjusted every 15 blocks to maintain the same detection level across the entire session. Target contrasts averaged across participants were 3.2 ± 0.45 %, 2.2 ± 0.27 %, 2.88 ± 0.38 %, for position 1, 2, and 3, respectively, for the 4 Hz-induced frequency; 3.35 ± 0.55 %, 2.02 ± 0.29 %, 2.68 ± 0.27 %, for position 1, 2, and 3, respectively, for 6 Hz; 3.16 ± 0.31 %, 2.1 ± 0.19 %, 2.55 ± 0.18 %, for position 1, 2, and 3, respectively, for 8 Hz; and 3.03 ± 0.31 %, 2.02 ± 0.17 %, 2.45 ± 0.16 %, for position 1, 2, and 3, respectively, for 10 Hz.

EEG Analysis

Analyses were performed with EEGLab 13.6.5 (Delorme and Makeig, 2004; Swartz Center for Computational Neuroscience, UC San Diego, California) running in Matlab.

Preprocessing. EEG data and channel location were imported into EEGLab. EEG data were re-referenced to the average of the right and left mastoids. A high-pass filter at 0.1 Hz and a notch filter between 48 and 52 Hz were applied, to respectively remove slow drifts and 50 Hz electric noise. The signal was further down sampled to 512 Hz. Visual inspection allowed to identify electrodes with low signal-to-noise ratio, which were then interpolated (spherical interpolation). Independent component analysis (ICA) was performed to remove blink

components, after a visual inspection of their time courses and topographies. Data were epoched from trial onset (0s) to the end of the block (+30s).

Fast Fourier Transform. FFT were computed (Matlab function: fft) on 30s-epoched EEG data, and the amplitude was extracted for each electrode, epoch, and frequency. The signal-to-noise ratio (SNR) was computed on the amplitude extracted from the FFT, for each electrode, as the ratio of the amplitude at each frequency to the average of the 20 surroundings frequencies (10 frequencies on either side, excluding the immediately adjacent frequencies; note that the SNR could mathematically not be estimated at the edges of the spectra), as described in Rossion et al. (2012) and Liu-Shang et al. (2014). SNR averaged across participants, epochs and electrodes were plotted to ensure that the oscillating disk successfully induced brain signal at the corresponding frequency. Topographies were plotted at the peak of the induced frequency and its first harmonic.

Event-Related Potentials (ERPs). Previously preprocessed EEG timeseries were further bandpass filtered between 1.5 Hz and 30 Hz, and baseline corrected from -400 to 0 ms from block onset. Epochs of one second were defined (time-locked to full-black disk), excluding the first second of each 30 seconds-block to avoid the transient EEG response due to stimulus onset. Participants' ERPs were computed as the averaged of all resulting epochs. ERPs averaged across participants for electrode Oz were plotted with the standard error of the mean. Electrode Oz was selected because it is the electrode with the highest amplitude across the four induced frequencies. The ERP plots allowed us to identify that the brain oscillation induced by the oscillating disk was a complex oscillation, i.e., composed of two sinusoidal oscillations, one at the induced frequency and the second at its first harmonic. Therefore, a complex sine function was fitted to the behavioral data.

FFT on ERPs. FFT was computed (1500 points zero padding) on the 1s-Oz ERP for each participant. The amplitude was extracted, and the SNR was computed as previously described.

Behavioral analysis

Behavioral analyses were performed with Matlab R2014b (The MathWorks, Natick, MA). The following dependent variables were computed: hit rates as main dependent variable, i.e., percentage of correct responses, and median reaction times as secondary dependent variables, for each target position and frequency. Hit rates averaged across frequencies were 42.82 ± 3.45 %, 43.53 ± 3.22 %, and 41.77 ± 3.48 % for position 1, 2, and 3, respectively. Median reaction times averaged across frequencies were 511 ± 8 ms, 512 ± 8 ms, and 510 ± 9 ms for position 1, 2, and 3, respectively. A two-way repeated-measures ANOVA was performed for each dependent variable to assess the effect of frequency and target position. For hit rates, there was a main effect of target position ($F(2, 32) = 11.46$, SS = 236.74, p-value < 0.01, $eta^2 = 41.75$) but no effect of frequency ($F(3, 48) = 1.58$, SS = 76.31, p-value = 0.2, $eta^2 = 8.99$) nor of their interaction ($F(6, 96) = 0.36$, SS = 12.66, p-value = 0.9). For median reaction times, there was no main effect of frequency ($F(3, 48) = 2..8$, SS = 4093.43, p-value = 0.11, $eta^2 = 11.55$), nor main effect of target position ($F(2, 32) = 0.04$, SS = 12.38, p-value = 0.96, $eta^2 = 0.25$), nor of their interaction ($F(6, 96) = 1.02$, SS = 622.66, p-value = 0.41). The absence of significant interaction between frequency and target positions in any of these two tests confirm successful contrast manipulation, i.e., the detection performance does not rely on an interaction between frequency and target positions. As argued in Kienitz et al. (2022) and VanRullen and Dubois (2011), reaction time fluctuations do not unambiguously demonstrate rhythms in cognitive processes as they can also be the by-product of the external stimulation and are sensitive to changes in decision criteria (Reed, 1973; Wickelgren, 1977; Carrasco and McElree, 2001; Dugué et al., 2018, 2020). The behavioral phase analyses thus focused on hit rates as the main dependent variable.

Phase effect on detection performance. Each target was assigned to one of 7 phase bins of the periodic stimulation depending on the delay at which they appeared during the block. There were 124 blocks with on average 10 targets per block for each frequency, i.e., ~1240 trials per frequency in total, resulting in ~413 trials per position and ~60 trials per phase bin. Hit and false alarm rates were computed for each target position, frequency, and phase bin. For each

block and target position, false alarms (participants reported perceiving a target while no target had been presented; participants were instructed to respond in the 1s-window following the target, after which the response was considered a false alarm) were binned as a function of the phase of the oscillating disk. To allow for a fair comparison between hit and false alarms, only the false alarms that were in the same phase bins as the targets (but in a different 100-ms period) were considered for further analysis (e.g., if 2 targets were presented at position 1 within the given block, and binned in bins number 2 and 6, only false alarms that were binned in bins number 2 and 6 were considered for further analysis). To allocate a false alarm to one of the three target positions (a false alarm is, by definition, at none of the position), a bootstrap procedure was performed (100 repetitions).

Given the ERP results (see **Figure 2**) showing a complex neural response composed of the induced frequency and its first harmonic, a complex sine function was fitted to behavioral data (Eq1) with the following free parameters: $x[1]$ and $x[2]$ the amplitude and the phase offset of the induced frequency, respectively, $x[3]$ and $x[4]$ the amplitude and the phase offset of the first harmonic, respectively, and $x[5]$ the baseline level. To find the parameters that best fit the data, we used a Least Squares cost function, i.e., the cost function computed the total squared errors, i.e., the sum of squared errors, between the fit and the data, thus giving a measure of how well the data are fitted. The best fit is the one whose parameters minimize the total error (Watt et al., 2020).

$$(Eq1)\ \ x[1] * \big(sin(2 * \pi * T + x[2])\big) + \ x[3] * (sin\left(2 * \pi * \frac{T}{2} + x[4]\right)) + \ x[5]$$

We then performed a Monte Carlo procedure on the fitted amplitude (see **Statistical Analyses** section) to evaluate whether the fitted data was modulated periodically as a function of the phase. Note that false alarms were low in each phase bins (< 0.5%) and not significantly modulated periodically after Bonferroni correction across frequencies and positions (p-value threshold < 0.01, corresponding to a Z-score threshold of 2.64, and a Cohen's d threshold of 1.66). Consequently, in the next steps of the analysis, only hit rates were considered.

A group level analysis was also performed. Empirical and surrogate data were averaged across participants, and the same Monte Carlo procedure was performed.

Variance explained by the spatial organization of targets. We hypothesized that the spatial organization of brain oscillations should explain a larger variance in the behavioral phase effect. To test this hypothesis, the hit rate was computed for each frequency and phase bin, regardless of target position. The complex sine function was then fitted to the hit rate (Eq1) and the amplitude modulation, i.e., difference in hit rate between the optimal and the non-optimal phase, was computed for each frequency and participant. Two-tailed t-tests were used to assess whether the amplitude modulation averaged across the three target positions was significantly different than the amplitude modulation computed across targets independently of their position, for each frequency.

Optimal phase shift between target positions for each induced brain oscillation. The optimal phase, i.e., the position on the fitted curve at maximal performance, was extracted for each target position and frequency, on data averaged across participants and for each participant individually. We asked whether the optimal phase shift as a function of target positions was different between the four induced frequency conditions, i.e., whether there is a significant interaction between frequency and target position.

The optimal phases were converted in radians. A one-cycle sine wave was generated with the phase offset of the oscillating disk and phase values were extracted in radians along the entire cycle. The optimal phase extracted from data fitting was then calculated in radian based on this one-cycle sine wave fit participant-by-participant. We then obtained rose plots of all individual optimal phases with the function circ_plot from the Circular Statistics Toolbox (see **Figure 4**; P. Berens, CircStat: A Matlab Toolbox for Circular Statistics, Journal of Statistical Software, Volume 31, Issue 10, 2009, http://www.jstatsoft.org/v31/i10), for each frequency and target position. A Harrison-Kanji test was performed (two-way ANOVA for circular data; circ_hktest from the Circular Statistics Toolbox) on the individual optimal phases, with

frequency and position as factors. An interaction would indicate that the effect of position on the optimal phase differs across frequency conditions.

Post-hoc tests on optimal phases obtained allowed assessing which specific frequencies displayed a change in the optimal phase. The optimal phase in radians was compared between target positions by computing the pairwise phase difference with the function circ_dist from the Circular Statistics Toolbox. Statistics were performed with a Monte Carlo procedure ideal for the sample used in this study (Abraham and Russell, 2008) (see **Statistical analyses** section). To going further, we computed the pairwise phase difference with the function circ_dist participant-by-participant, for each pair of positions (positions 1 and 2, 1 and 3, 2 and 3), and we tested whether the pairwise phase difference was significantly different against 0, i.e., null difference, for each frequency and pair of positions, with a Watson-Williams test (function circ_wwtest) from the Circular Statistics Toolbox. P-value were Bonferroni corrected for multiple comparisons across target positions and frequencies (p-value threshold < 0.01). This analysis allowed to investigate whether the phase shift was systematic across participants.

Control experiment

Experimental Design The targets were of same size and location as in the main experiment. The peripheral disk was, however, not modulated sinusoidally but was flashed (during three frames, for a total of 6.3 ms) at 7 different levels of luminance (7 contrast levels: 5%, 20.8%, 36.7%, 52.5%, 68.3%, 84.2% and 100%) at the same time as target onset to test for luminance masking. There was 20% of catch trials in which the disk was flashed but not the target.

As for the main experiment, the control experiment first included a staircase procedure to adjust the contrast of each target, for each participant, to reach 50% detection. In 7 blocks, the luminance of the disk was set at 50% contrast. For each block, 6 to 18 targets were presented (~10 targets/trials per block on average), thus the staircase procedure contained an average of 70 trials.

Then, participants performed four runs of 38 blocks each in two separate experimental sessions of approximately 1h30 each (no EEG recording for this control experiment). Each

contrast level was displayed the same number of times (~217 targets per contrast level). Target contrasts were adjusted every 15 blocks to maintain the same detection level across the entire session.

Analyses. 47.5 ± 56.4 targets were rejected from the analysis due to blinks or saccade eye movements. Hit rates, i.e., percentage of correct detection, median reaction times and target contrasts were computed for each target position. Hit rates were 57.18 ± 1.1 %, 51.74 ± 0.35 %, and 45.82 ± 0.76 % for position 1, 2 and 3, respectively. Median reaction times were 474 ± 2 ms, 511 ± 3 ms, and 525 ± 3 ms, for position 1, 2, and 3, respectively. Target contrasts were 0.61 ± 0.01 %, 1.16 ± 0.04 %, and 0.71 ± 0.02 %, for position 1, 2, and 3, respectively. A one-way repeated-measures ANOVA was performed for each dependent variable to assess the effect of target position. For hit rates, there was no main effect of target position ($F(1,14) = 2.52$, p-value = 0.09, $eta^2 = 15.29$). For median reaction times, there was also no main effect of target position ($F(1,14) = 1.24$, p-value = 0.30, $eta^2 = 8.16$). The absence of a significant main effect of target positions in any of these two tests confirm successful contrast manipulation. For target contrast, there was a main effect of target position ($F(1,14) = 13.68$, p-value < 0.01, $eta^2 = 49.42$), which is coherent with the staircase manipulation.

Targets were binned according to the level of luminance of the simultaneously presented disk. To emulate an oscillatory cycle (which, in the main experiment, goes from 0% contrast to 100% and back to 0%), we used a bootstrap procedure (5 000 repetitions) randomly assigning half of the targets to one half of the cycle (from contrast 0% to 100%), while the other half was assigned to the second half of the cycle (from contrast 100% to 0%), thus resulting in 13 luminance levels.

The number of false alarms (i.e., participants responded a target was present while it was absent), and the number of hits were computed for each target position and for the 13 luminance levels. A one-cycle sine function was fitted to individual data and data averaged across participants (Eq2) with the following free parameters: the amplitude, $x[1]$, the phase

offset, $x[2]$, the baseline, $x[3]$, and a Least Squares cost function was used to find the parameters that best fit the data.

$$(Eq2)\ \ (x[1] * \big(sin(2 * \pi * T + x[2])\big) + \ x[3]$$

We performed a Monte Carlo procedure on the fitted amplitudes to assess whether the fitted data was modulated periodically by the luminance disk (see **Statistical analyses** section). There was no significant effect of luminance, at any target position, for the false alarm ratio and thus we did not consider this variable any further.

The optimal phase, i.e., phase of highest performance, was computed for each target position on data averaged across participants. To study whether the optimal phase shifted as a function of target positions, we computed the pairwise phase difference and assessed the significance using a Monte Carlo procedure (see **Statistical analyses** section).

Statistical Analyses

To test whether the fitted data was significantly modulated periodically by the phase of the oscillating disk (see **Phase effect on detection performance** section*)*, a Monte Carlo procedure on the fitted amplitude was performed. 50,000 surrogates were generated for each participant, target position and frequency, by randomly assigning correct responses, i.e., for each target, we randomly assigned an incorrect or a correct response based on the averaged performance, and false alarms, i.e., a number of false alarms at an associated random delay was randomly assigned to each block, based on the average number of false alarms throughout the experiment. Hit and false alarm rates were then computed for each phase bin, position, and frequency, and the same sine function were fitted (Eq1). The surrogate distributions of the 50,000 fitted amplitudes for the induced frequency and its first harmonic separately were compared to the empirical fitted amplitudes. P-values were obtained by computing the proportion of fitted amplitudes equal or higher than the empirical fitted amplitude (fitted amplitudes: free parameters $x[1]$ and $x[3]$ from (Eq1)). The fitted amplitudes of the induced frequency ($x[1]$) and of the first harmonic ($x[3]$) across all frequencies and target

positions were compared with two-tailed t-test to investigate which frequency contribute the most to the oscillatory pattern.

A similar Monte Carlo procedure was performed to test for a significant difference of the optimal phases between target positions (see **Optimal phase shift between target positions for each induced brain oscillation** section). 50,000 datasets were created for each target position and frequency, by randomly assigning detection performance according to the average values for each pair of positions (positions 1 and 2, 1 and 3, 2 and 3), and by considering the original distribution of the number of targets across participants and phase bins. The sine function (Eq1) was fitted to the data. The optimal phase was computed and converted in radians, and the phase difference was obtained for each pair of position. Thus, we obtained a surrogate of 50 000 phase differences for each pair of positions and each frequency. By computing the proportion of surrogate phase difference equal or higher than the real phase difference, we obtained p-values.

P-values were Bonferroni corrected for multiple comparisons across target positions and frequencies (p-value threshold of 0.01).

In the control experiment (see **Control experiment** section), the same Bonferroni corrected Monte Carlo procedures were performed, except that the 50,000 datasets were created for each luminance values (instead of phase bins) and that the sine function (Eq2) was fitted to the data.

Code Accessibility

Raw behavioral data and code relative to the main results will be available at https://github.com/CamilleFakche after publication.

Results

Participants (n=17) performed a threshold visual detection task, while a luminance oscillating disk was concurrently presented in the periphery (eccentricity: 7.5°) to induce theta/alpha brain

oscillations (4, 6, 8 and 10 Hz; EEG simultaneously recorded). Near-threshold target stimuli appeared at one of three possible eccentricities between a central fixation cross and the disk (**Figure 1A**; adjusted according to cortical magnification so each target measured 0.8 mm of diameter and were placed 0.8 mm away from each other in the cortex; see **Figure 1B**). We tested whether (1) the periodic disk stimulation modulates detection performance periodically at each target position, (2) the optimal phase (of highest performance) shifts as a function of distance from the disk suggesting that perceptual cycles travel across space (**Figure 1C**), and (3) the occurrence of such traveling properties depends on the induced frequency.

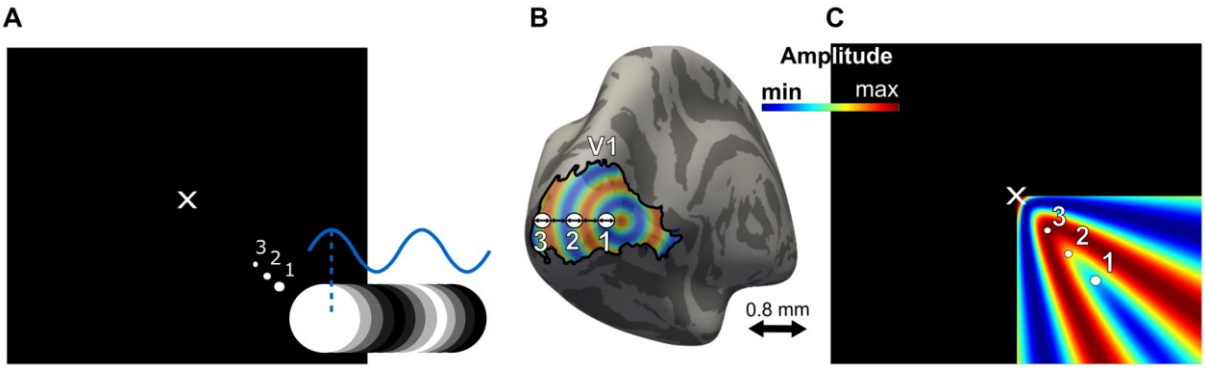

Figure 1. Experimental protocol. A. *A luminance oscillating disk (inducer) was presented in the periphery to induce brain oscillations in the visual cortex (e.g., V1). Participants were instructed to detect visual targets at threshold (50% detection) at three different positions in the retinotopic space, based on cortical magnification. Disks oscillated for a 30-seconds period during which 6 to 18 targets were presented at random times according to a decreasing probability distribution. Participants pressed the space bar when they detected the target (1-s response window after target onset)* ***B.*** *In the visual cortex, visual targets measured 0.8 mm of diameter and were placed 0.8 mm away from each other.* ***C.*** *Hypothesis: the oscillating disk, presented in the lower right corner, induced a brain oscillation that traveled across the retinotopic space (note that we concentrate our predictions to the quadrant in which the disk is presented). At an instant t, position 3 is located at the optimal phase of the oscillation (leading to the highest performance, i.e., max Amplitude), while position 1 is located at the non-optimal phase (i.e., min Amplitude).*

EEG activity was analyzed using frequency decomposition (Fast Fourier Transform, FFT, performed on the time series of each participant and electrode) and Event-Related Potentials (ERPs) measures to ensure that we successfully induced brain oscillations and to characterize

411 the shape of the evoked response. First, peaks in the spectrum (as measured per SNR,
412 averaged across participants and electrodes) were identified for each induced frequency (4, 6,
413 8 and 10 Hz; SNR > 1.4) and their first harmonics (8, 12, 16 and 20 Hz; SNR > 1.57), with
414 topographies showing brain activity in the occipital cortex (for simplicity, frequencies were
415 rounded to a whole number; real values are displayed in **Figure 2 left side of each panel**).
416 Second, ERP analyses showed that the evoked signal is a complex oscillation composed of
417 the induced frequency and its first harmonic (**Figure 2 right side of each panel**). We further
418 computed an FFT on the ERPs of electrode Oz. Peaks were again identified for each induced
419 frequency (4, 6, 8 and 10 Hz; SNR > 2.4) and their first harmonics (8, 12, 16 and 20 Hz; SNR
420 > 4.41; data not shown). These complex evoked responses were interpreted as the overlap
421 between the periodic brain response (i.e., inducer) and the neural population response to
422 individual stimuli (i.e., contrast change) at low frequencies, or alternatively, to the nonlinear
423 nature of the visual system, i.e., nonlinear systems produce complex output consisting of the
424 input frequency and multiple harmonics (Heinrich, 2010; Norcia et al., 2015). Together, the
425 EEG analyses confirm that we successfully induced theta/alpha oscillations in the visual cortex
426 and show that the evoked signal is a complex oscillation composed of the induced frequency
427 and its first harmonic (Heinrich, 2010; Norcia et al., 2015).

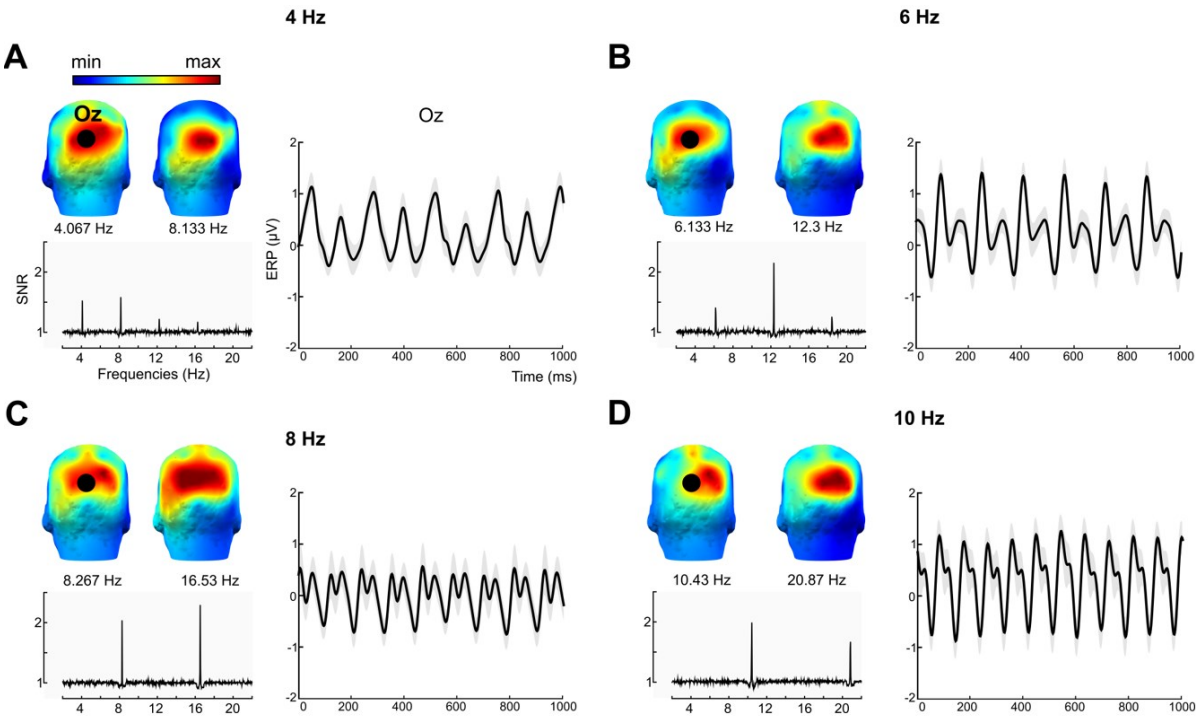

Figure 2. The oscillating disk evokes complex brain oscillations in the occipital cortex. *Left side of each panel, Fast Fourier Transform analyses performed on the EEG time series. Right side of each panel, ERP analyses, for induced frequencies of* ***A.*** *4,* ***B.*** *6,* ***C.*** *8 and* ***D.*** *10 Hz (rounded frequency values). Signal-to-noise ratio (SNR) amplitude averaged across 17 participants and all 62 electrodes, from 2 to 22 Hz. In each panel, a peak in SNR is identified for the induced frequency and its first harmonic. Topographies of the two SNR peaks revealed that we successfully induced brain oscillations in the visual cortex. Black dot, Electrode Oz. ERP of the Oz electrode computed on one-second epochs (the first-second epoch was removed to each 30-seconds blocks to avoid the EEG transient evoked response; each block represented 29 1-second epochs) averaged across participants (n=17). Solid black line, averaged ERP. Shaded area, standard error of the mean.*

Second, we investigated whether detection performance was modulated periodically for each induced frequency and each target position. Targets (from 6 to 18 targets per 30 seconds-blocks) can appear at random delays during the periodic disk stimulation (from 1s to 29s from disk onset). Targets were binned according to the phase of the oscillating disk (7 bins/cycle; least number of bins to sample one oscillatory period while allowing a large number of trials per bin to achieve high statistical power). In each bin, detection performance was computed as per hit rate (correct target detection) for each participant, frequency, and target position. Finally, the data were averaged across participants and, given the complex shape of the ERP

(**Figure 2**), fit to a complex sine function, separately for each frequency and target position. Detection performance showed a significant oscillatory pattern for each target position and frequency (Monte Carlo on fitted amplitude, Bonferroni corrected across frequencies and positions, p-value threshold < 0.01, corresponding to a Z-score threshold of 2.64, and a Cohen's d threshold of 1.66; **Figure 4**), and a clear optimal phase (of highest performance). Note that the fitted amplitude of the induced frequency was significantly higher than the one of the first harmonic (Two-tailed t-test on fitted amplitude across all frequencies and positions, p-value < 0.01, Cohen's d = 0.67, CI = [0.05; 0.1]), suggesting that the oscillatory pattern was mainly driven by the induced frequency. The inducer modulated detection performance periodically, at each target position and at each frequency, with an average amplitude modulation (optimal to non-optimal hit rate difference) of 42.71 ± 3.37 %. The amplitude modulation was further computed for each participant, frequency, and target position (**Figure 3**). A two-way repeated-measures ANOVA revealed a significant main effect of the frequency ($F(3, 48) = 23.85$, SS = 0.67, p-value < 0.01, $eta^2 = 59.85$), and no main effect of the target position ($F(2, 32) = 0.9$, SS = 0.01, p-value = 0.41, $eta^2 = 5.33$), nor of the interaction ($F(6, 96) = 0.92$, SS = 0.03, p-value = 0.48). The amplitude modulation was of 49.84 ± 3.45% for 4 Hz, 46.56 ± 3.57 % for 6 Hz, 39.04 ± 2.67 % for 8 Hz, and 35.39 ± 2.54 % for 10 Hz. Post-hoc two-tailed t-tests showed that the amplitude modulation was higher for 4 Hz compared to 8 Hz (p-value < 0.01, Cohen's d = 0.84, CI = [0.07; 0.14]) and 10 Hz (p-value < 0.01, Cohen's d = 1.15, CI = [0.1; 0.18]), with a tendency compared to 6 Hz (p-value = 0.06, Cohen's d = 0.22, CI = [-0.01; 0.06]), higher for 6 Hz compared to 8 Hz (p-value < 0.01, Cohen's d = 0.57, CI = [0.04; 0.1]) and 10 Hz (p-value < 0.01, Cohen's d = 0.87, CI = [0.07; 0.14]), and higher for 8 Hz compared to 10 Hz (p-value = 0.02, Cohen's d = 0.33, CI = [0.01; 0.06]). In summary, the amplitude modulation decreases with increasing frequency but is constant across target positions. The amplitude modulation allowed to reliably estimate the optimal phase at each frequency and target positions. A complementary analysis showed that behavioral performance was better explained when taking into account the spatial position of the targets. Specifically, we compared the amplitude modulation when detection performance was

calculated disregarding target position, with the amplitude modulation calculated independently for each target position and then averaged across positions (two-tailed t-tests Bonferroni corrected for multiple comparisons: 4 Hz, t-stat = -5.99, p-value < 0.01, Cohen's d = -0.3, CI = [-0.05; -0.02]; 6 Hz, t-stat = -5.24, p-value < 0.01, Cohen's d = -0.25, CI = [-0.04; -0.02]; 8 Hz, t-stat = -5.44, p-value < 0.01, Cohen's d = -0.3, CI = [-0.04, -0.02]; 10 Hz, t-stat = -9.2, p-value < 0.01, Cohen's d = -0.52, CI = [-0.05; -0.03]). The amplitude modulation was significantly stronger when calculated position-by-position, suggesting that taking into account the spatial position of visual targets better explain perceptual performance.

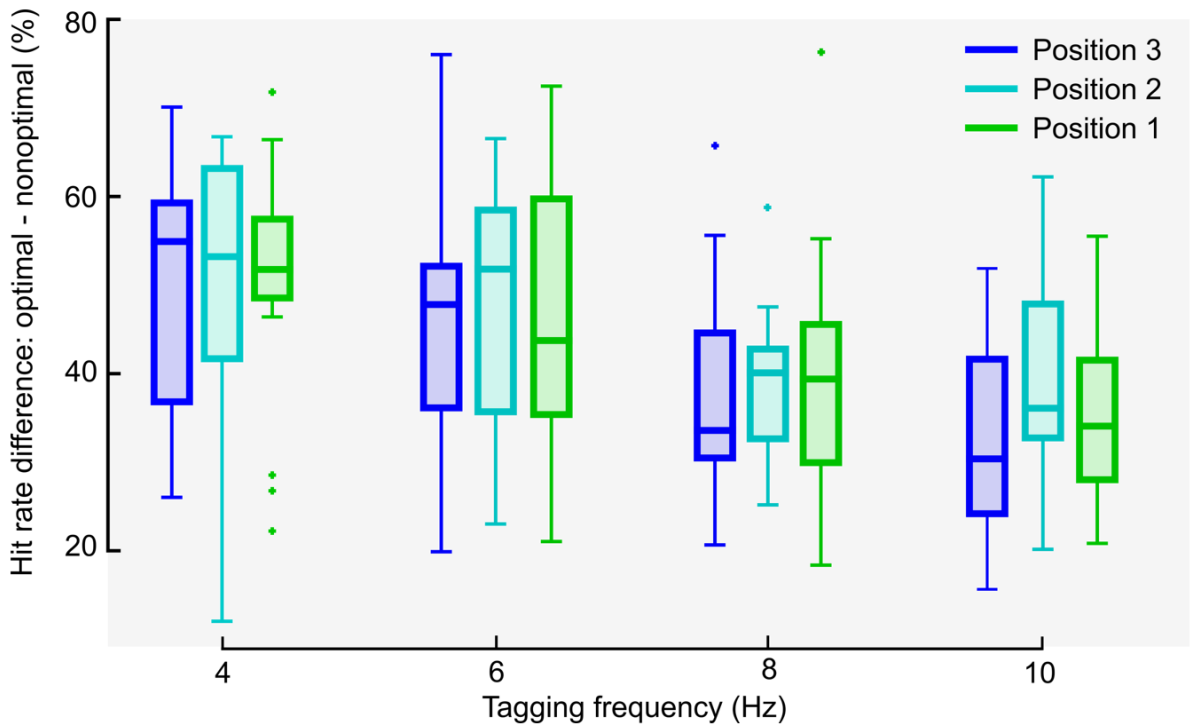

Figure 3. The amplitude modulation decreased with increasing induced frequency. *Amplitude computed as the difference between the maximum and the minimum hit rate. Dots, individual outlier data. A two-way repeated-measures ANOVA revealed a significant main effect of frequency (F(3, 48) = 23.85, SS = 0.67, p-value < 0.01, eta² = 59.85).*

Critically, we tested whether (1) perceptual cycles propagate across the retinotopic space, and (2) the occurrence of such traveling properties depends on the induced frequency. Propagation is defined as a shift in the optimal phase between two positions. To assess whether the optimal phase shifted as a function of target position, individual optimal phases were converted in

radians based on a one-cycle sine wave fit (see **Methods**) at the induced frequency (the oscillatory pattern was mainly driven by the induced frequency; see analysis above). A Harrison-Kanji test revealed a significant main effect of the frequency ($F(3,48) = 25.13$, SS = 14.33, p-value < 0.01), target position ($F(2,32) = 3.06$, SS = 1.16, p-value = 0.04) and a tendency for the interaction ($F(6,96) = 1.99$, SS = 2.42, p-value = 0.06). Post-hoc analyses on the optimal phase difference (reported in degrees for easier readability of **Figure 4**) between each pair of target positions (1 and 3, 1 and 2, and 2 and 3; Monte Carlo, Bonferroni corrected across frequencies and positions, p-value threshold < 0.01, corresponding to Z-score threshold of 2.64, and a Cohen's d threshold of 1.66) revealed a significant phase shift between positions 1 and 2, and 1 and 3 for 8 Hz- and 10 Hz-induced frequencies (**Figure 4C,D**). We found no significant phase shift for 4 Hz- and 6 Hz-induced frequencies (**Figure 4A,B**). To further confirm the previous results, we performed Watson-Williams tests against 0, i.e., null difference, on pairwise phase difference computed participant-by-participant, for each pair of positions (positions 1 and 2, 1 and 3, 2 and 3), for the 8 Hz- and 10 Hz-induced frequency conditions. The results showed a significant phase shift between positions 1 and 2, 1 and 3, and 2 and 3, for both 8 Hz and 10 Hz (Bonferroni corrected across frequencies and positions, p-value < 0.01). Compared to the Monte Carlo procedure, the Watson-Williams tests are tailored to take into account the inter-variability across participants. Even then, we found that the optimal phase systematically and significantly shifts between each position in the visual field. Together, the results demonstrate that the optimal phase of alpha perceptual cycles shifted across target positions, suggesting that the alpha-induced oscillations traveled across the retinotopic cortical space.

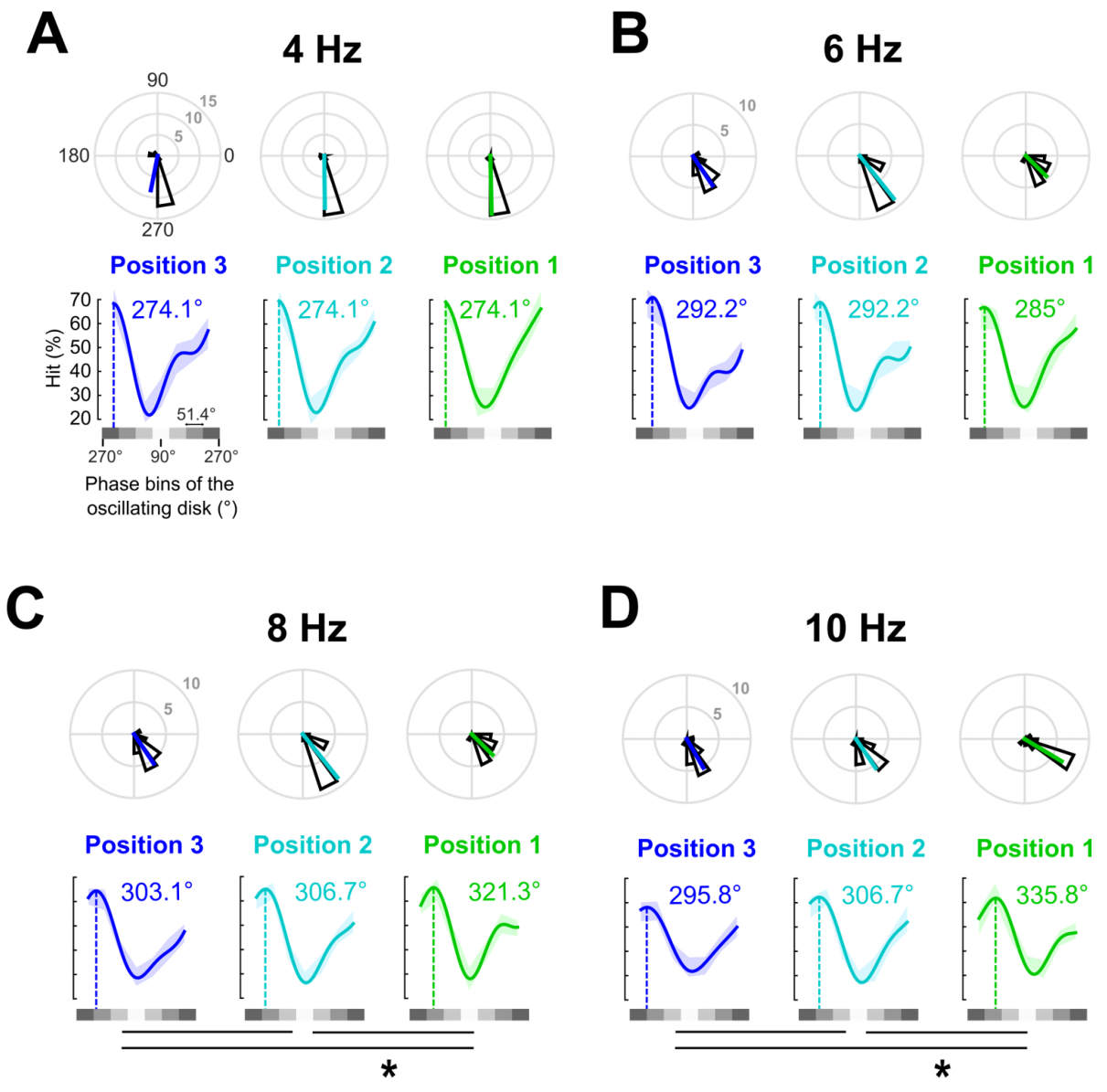

Figure 4. The optimal phase of alpha perceptual cycles shifts between target positions. *Lower graph of each panel, hit rate averaged across participants (n=17), binned as a function of the phase of the oscillating disk, and fitted to a complex sine function. Shaded colored area, 95 confidence intervals. Solid line, sine fit. Dotted line, optimal phase in degrees. The value of the optimal phase in degrees is extracted for fit on data averaged across participants (note that this closely resemble the value obtained from averaging individual optimal phases from top graph). Top graph of each panel, rose plot distribution of the optimal phase across participants. Colored solid line, optimal phase averaged across participants. Gray scale, phase bins of the oscillating disk (90°, white disk). Each bin represents 51.4° of the oscillatory cycle.* ***A.*** *results for induced frequencies of* ***A.*** *4,* ***B.*** *6,* ***C.*** *8 and* ***D.*** *10 Hz. Performance was significantly modulated periodically at each target position and frequency (Monte Carlo, Bonferroni corrected across target positions and frequencies, p-value threshold < 0.01). The*

optimal phase shifted between positions 1 and 2, 2 and 3, and 1 and 3 for 8 Hz- and 10 Hz-induced frequencies (Watson-William test, Bonferroni corrected across target positions and frequencies, p-value threshold < 0.01). There was no significant phase shift for 4 Hz- and 6 Hz-induced frequencies.

When converting the phase shift observed between target positions into milliseconds (3 ms for 8 Hz, and 5.5 ms for 10 Hz, respectively) and given the cortical distance between two target positions (0.8 mm distance edge-to-edge) as well as the targets' cortical size (0.8 mm diameter), one can estimate that alpha-induced brain oscillations traveled across the retinotopic space at an averaged propagation speed ranging between 0.3 (1.6 mm / 5.5 ms) and 0.5 m/s (1.6 mm / 3 ms).

Finally, one may ask whether the phase shift observed in behavioral data was due to luminance masking from the disk. We thus performed a control experiment on 15 participants to address this potential concern. Here, participants were instructed to detect visual targets at threshold (50% detection) at one of the same three positions as in the main experiment, while a peripheral disk was simultaneously flashed at one of seven possible levels of luminance. Detection performance showed a significant oscillatory pattern at each target position (Monte Carlo, Bonferroni corrected across positions, p-value threshold of 0.01, corresponding to a Z-score threshold of 2.12, and a Cohen's d threshold of 1.31, **Figure 5**) confirming the presence of luminance masking for all three positions. Importantly, however, seven participants took part in both the main and the control experiment. For these participants, we overlapped in **Figure 5B-H** the sine fits from the control experiment and from the 10 Hz-induced frequency from the main experiment. The oscillatory patterns clearly differed between the two experiments. If the phase effect was only due to masking, the optimal phase should be observed at 0% of contrast in the main experiment as it is the case for the contrast experiment, but this is not the case. More crucially, unlike in the main experiment, in the control experiment no phase shift between positions was found (p-value = 1, i.e., the pairwise phase differences were the same between the empirical and surrogate datasets).

Consequently, the phase shift cannot merely be explained by low-level luminance masking as confirmed with a control experiment (**Figure 5**) nor by a decreased phase estimation accuracy at low frequencies (see **Figure 3,** showing that the amplitude modulation is in fact higher at low compared to high induced frequency).

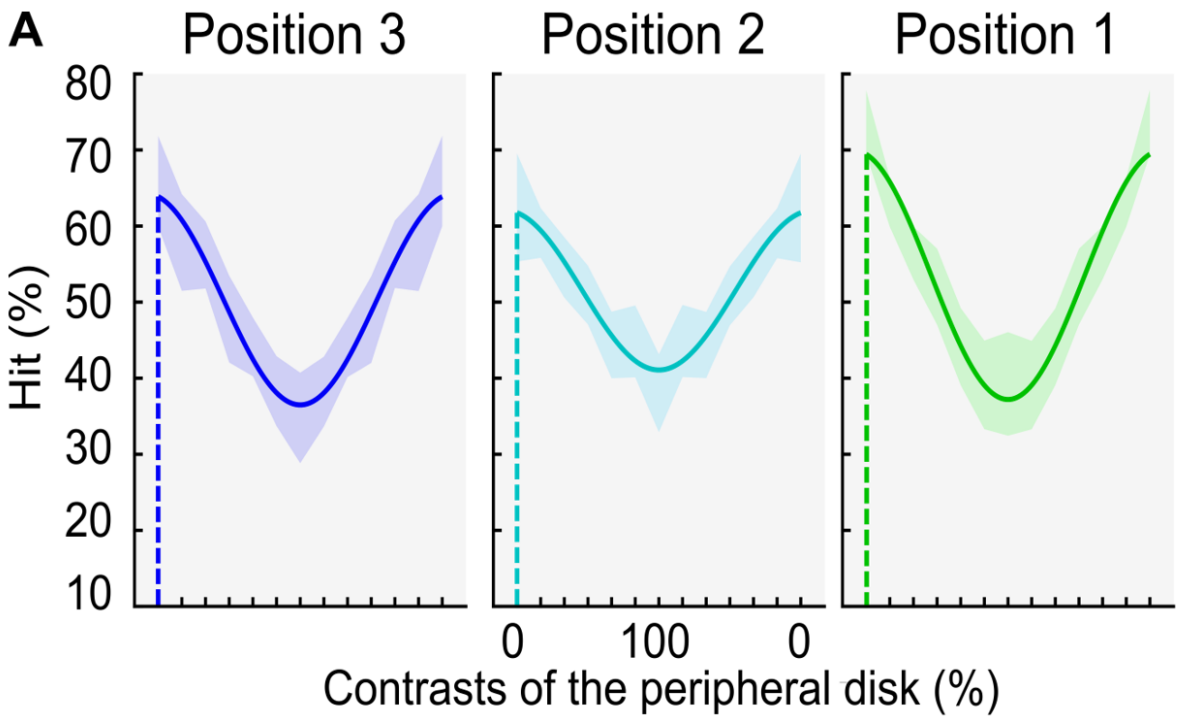

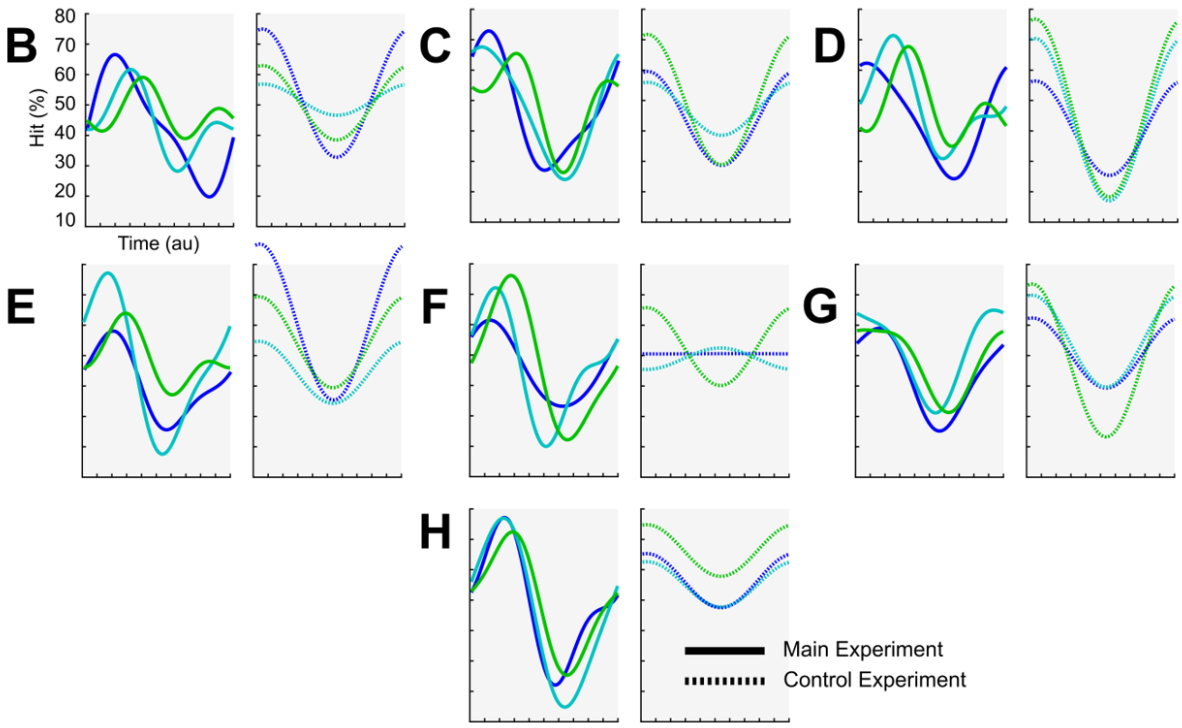

562 ***Figure 5. The propagation of perceptual cycles was not due to luminance masking. A.***
563 *Hit rate for each 13 luminance levels and the 3 target positions averaged across participants*
564 *(n=15) and fitted to a one-cycle sine function. Shaded colored area, 95 confidence intervals.*
565 *Solid line, fit. Dotted line, optimal phase.* ***B – H*** *Results from individual participants for the main*
566 *experiment on the left and the control Experiment on the right. Green, position 1. Cyan, position*
567 *2. Blue, position 3.*

568 **Discussion** (1500/1500)

569 Using psychophysics and EEG, the results showed that visual perception at each target
570 position is modulated periodically at the induced frequency, replicating previous results
571 (Stefanics et al., 2010; Mathewson et al., 2012; Henry and Obleser, 2012; Graaf et al., 2013;
572 Henry et al., 2014; Spaak et al., 2014; ten Oever and Sack, 2015; Kizuk and Mathewson,
573 2017). Critically, the optimal phase for visual perception systematically shifted between target
574 position. This effect was observed for alpha frequencies (8 Hz and 10 Hz; and cannot be simply
575 explained by a mere luminance masking confound) and not theta, with an average propagation
576 speed ranging from 0.3 to 0.5 m/s. Together, the results support the hypothesis that alpha-
577 induced brain oscillations travel across the visual cortex to modulate performance periodically
578 across space and time.

579 *Neural traveling waves, a growing, yet largely understudied field.* A traveling wave is the
580 propagation of neural activity over space with a monotonic shift in the peak latency between
581 the origin of the signal and more distal positions (Sato et al., 2012; Muller et al., 2018).

582 Mesoscopic waves travel *within* individual brain regions (e.g., V1) spanning millimeters, while
583 macroscopic waves travel *between* cortical areas (Sato et al., 2012; Muller et al., 2018).
584 Studies using invasive recordings with high spatial and temporal resolution showed non-
585 oscillatory traveling activity in visual cortices of mammals (Bringuier et al., 1999; Jancke et al.,
586 2004; Roland et al., 2006; Lippert et al., 2007; Sharon et al., 2007; Xu et al., 2007; Takagaki
587 et al., 2008; Nauhaus et al., 2009, 2012; Gao et al., 2012; Rekauzke et al., 2016; Slovin et al.,
588 2002; Chen et al., 2006; Sit et al., 2009; Reynaud et al., 2012; Zhang et al., 2012; Yang et al.,
589 2015; Chemla et al., 2019). Much fewer studies have focused on mesoscopic *oscillatory*

590 traveling waves. They showed that delta, theta, alpha, beta and gamma oscillations can
591 propagate within individual visual areas of mammals and turtles (Prechtl et al., 1997, 2000;
592 Sanchez-Vives and McCormick, 2000; Huang et al., 2004; Benucci et al., 2007; Han et al.,
593 2008; Ray and Maunsell, 2011; Maris et al., 2013; Stroh et al., 2013; Muller et al., 2014;
594 Townsend et al., 2015; Zanos et al., 2015; Davis et al., 2020). In humans, only a few studies,
595 using invasive recordings in patients, showed the propagation of theta, alpha, and beta
596 mesoscopic traveling waves (Takahashi et al., 2011; Zhang and Jacobs, 2015; Sreekumar et
597 al., 2021), but only in non-visual cortical areas. There is no electro-physiological study to date
598 investigating the propagation of low-frequency oscillations in individual human visual areas.

599 Finally, if a few studies have investigated the functional role of propagating oscillatory activity
600 at the mesoscopic levels (attention: Maris et al., 2013; memory: Han et al., 2008; motricity:
601 Rubino et al., 2006; Takahashi et al., 2011, 2015; saccadic eye movements: Zanos et al., 2015;
602 visual perception: Besserve et al., 2015; Davis et al., 2020), very little is known about the link
603 between oscillatory activity propagation within individual visual areas and perceptual
604 performance, especially in human. The present study addresses this clear gap in the literature.

605 *Oscillatory Mesoscopic Traveling Waves in visual areas have clear perceptual consequences.*
606 Sokoliuk and VanRullen (2016) reasoned that if an induced-oscillation propagates across the
607 visual cortex, it should have perceptual consequences across the retinotopic visual space.
608 Using a similar psychophysical paradigm, they found a shift of the behavioral optimal phase
609 as a function of distance from the inducer. Yet, there are two notable differences between their
610 study and the present one. First, they observed that the phase shifted between the visual
611 stimulus the closest to the inducer and more distant ones (no differences between intermediate
612 positions). Yet, postulating a wave is traveling within the cortex requires showing a phase
613 change across all positions. Here, contrary to Sokoliuk and VanRullen (2016), we found a
614 systematic phase shift across all three positions.

Second, Sokoliuk and VanRullen (2016) observed an optimal phase shift for both frequencies of 5 Hz (theta) and 10 Hz (alpha), but not 15 Hz. Here, however, we showed a shift for alpha-induced frequencies (8 Hz and 10 Hz), but not theta (4 Hz and 6 Hz).

Together, these discrepant results can be explained by a number of critical differences between the two studies. First, our EEG results revealed that the oscillating disk produced a complex neural response composed of the induced frequency and its first harmonic, coherent with the nature of the visual system (Heinrich et al., 2010; Norcia et al., 2015; Spaak et al., 2014). Thus, one must fit the behavioral response with a corresponding complex sine function to accurately capture the non-linearity of the neural response. Since the EEG was not recorded in Sokoliuk and VanRullen (2016), the shape of the induced-oscillation was unknown. Second, to ensure that the three targets activated the same number neurons in visual regions, hence landing in a similar spatial extent (spatial phase) of the traveling wave, we adjusted the size of each target to cortical magnification. Third, in our study, the same participants (n=17) performed all four frequency conditions thus ensuring equal statistical power and no inter-individual variability (n=5 for 5Hz, n=7 for 10Hz and n=15 for a 10-Hz replication set, and n=4 for 15Hz in Sokoliuk and VanRullen, 2016). Finally, we used eye-tracking to ensure stable fixation, critical when investigating retinotopic propagation.

Propagation of alpha but not theta oscillations. Attention is the cognitive function that selects relevant information to facilitate its processing while still being able to flexibly redeploy resources to other information if necessary (Carrasco, 2011; Dugué et al., 2018, 2020). Studies have shown that when covert attention (no head/eye movements) is sustained at a given spatial location, information is sampled periodically at the alpha frequency (review: Dugué and VanRullen, 2017; Kienitz et al., 2022). In other words, visual performance fluctuates over time along with the phase of alpha oscillations in detection tasks in which the target stimulus appeared always at the same spatial location (Valera et al., 1981; Busch et al., 2009; Mathewson et al., 2009; Busch and VanRullen, 2010; Dugué et al., 2011; Samaha and Postle, 2015; Samaha et al., 2017; Fakche et al., 2022). However, when multiple stimuli are presented,

642 attention rhythmically samples information at the theta frequency (Dugué et al., 2015; Landau
643 et al., 2012; Fiebelkorn et al., 2013; Song et al., 2014; Huang et al., 2015; Dugué et al., 2019;
644 Merholz et al., 2022; review: VanRullen, 2016; Dugué and VanRullen, 2017; Kienitz et al.,
645 2022; Keitel et al., 2022).

646 Here, while we did not explicitly manipulate covert attention, participants fixated at the center
647 of the screen and targets appeared in a constrained location suggesting that covert, voluntary
648 spatial attention was sustained on the bottom right quadrant. This manipulation likely recruited
649 alpha sampling, which potentially favored the propagation of alpha-induced oscillations
650 (although alpha-induced oscillations could also potentially travel in the absence of attention).
651 One can speculate that the propagation of alpha oscillations away from the main attention
652 focus could allow the observer to periodically monitor other nearby locations allowing for
653 flexible attentional reallocation when a target appears. Further studies are necessary to
654 investigate this hypothesis.

655 Note that, here, we used a disk oscillating in luminance to induce brain oscillations and thus
656 facilitate the test of our traveling wave hypothesis. It is still, however, debated whether such
657 stimulus does in fact induce a *true* brain oscillation or a simple succession of ERPs. Critically,
658 the propagation of perceptual cycles we observed in this study is frequency band-specific
659 speaking in favor of the involvement of brain oscillations as the most parsimonious
660 interpretation. Regardless, whether an oscillation or an ERP, the results show propagation.
661 Future investigations will aim to disentangle these two alternatives.

662 *Speed and spatial extent of mesoscopic traveling waves*. Our results show that alpha waves
663 travel across the retinotopic space at a propagation speed ranging from 0.3 to 0.5 m/s. Such
664 observation is in line with results from the animal literature showing that low-frequency
665 oscillations propagate within visual areas at a speed ranging from 0.01 to 0.6 m/s (Prechtl et
666 al., 1997, 2000; Sanchez-Vives and McCormick, 2000; Benucci et al., 2007; Han et al., 2008;
667 Ray and Maunsell, 2011; Muller et al., 2014; Zanos et al., 2015; Davis et al., 2020).
668 Additionally, given a phase difference of maximum 40° between target positions, it is unlikely

669 that more than one (spatial) cycle (360°) of oscillatory activity propagates across such a small
670 portion of the visual cortex, in line with previous observations (Zanos et al., 2015; Zhang and
671 Jacobs, 2015).

672 Finally, given our specific contrast manipulation and the observed propagation of perceptual
673 cycles, it is likely that our paradigm preferentially probed alpha traveling waves in area V1 (with
674 small receptive fields).

675 *Conclusion*. Using a carefully designed psychophysical paradigm, combined with EEG and
676 eye-tracking, our study demonstrates that alpha perceptual cycles travel across the retinotopic
677 visual space in humans, at a propagation speed ranging from 0.3 to 0.5 m/s. These results
678 suggest that alpha-induced brain oscillations travel across the visual cortex to modulate
679 performance periodically across space and time.

680 References

681 Abraham W T, and Russell D W (2008) Statistical power analysis in psychological research.
682 Social and Personality Psychology Compass 2(1): 283-301.

683 Baumgarten TJ, Schnitzler A, and Lange J (2015) Beta oscillations define discrete perceptual
684 cycles in the somatosensory domain. PNAS 112: 12187–12192.

685 Benucci A, Frazor RA, and Carandini M (2007) Standing waves and traveling waves
686 distinguish two circuits in visual cortex. Neuron 55: 103–117.

687 Berens P (2009) CircStat: A MATLAB Toolbox for Circular Statistics. Journal of Statistical
688 Software 31: 1–21.

689 Besserve M, Lowe SC, Logothetis NK, Schölkopf B, and Panzeri S (2015) Shifts of gamma
690 phase across primary visual cortical sites reflect dynamic stimulus-modulated information
691 transfer. PLOS Biology 13, e1002257: 1-29.

692 Bringuier V, Chavane F, Glaeser L, and Frégnac Y (1999) Horizontal propagation of visual
693 activity in the synaptic integration field of area 17 neurons. Science 283: 695–699.

694 Busch NA, and VanRullen R (2010) Spontaneous EEG oscillations reveal periodic sampling
695 of visual attention. PNAS 107: 16048–16053.

696 Busch NA, Dubois J, and VanRullen R (2009) The phase of ongoing EEG oscillations predicts
697 visual perception. J Neurosci 29: 7869–7876.

698 Carrasco M (2011) Visual attention: The past 25 years. Vision Research 51: 1484–1525.

699 Carrasco M, and McElree B (2001) Covert attention accelerates the rate of visual information
700 processing. PNAS 98: 5363–5367.

701 Chemla S, Reynaud A, Volo M di, Zerlaut Y, Perrinet L, Destexhe A, and Chavane F (2019)
702 Suppressive traveling waves shape representations of illusory motion in primary visual cortex
703 of awake primate. J Neurosci 39: 4282–4298.

Chen Y, Geisler WS, and Seidemann E (2006) Optimal decoding of correlated neural population responses in the primate visual cortex. Nat Neurosci 9: 1412–1420.

Davis ZW, Muller L, Martinez-Trujillo J, Sejnowski T, and Reynolds JH (2020) Spontaneous travelling cortical waves gate perception in behaving primates. Nature 587: 432–436.

Delorme A, and Makeig S (2004) EEGLAB: an open source toolbox for analysis of single-trial EEG dynamics including independent component analysis. J Neurosci Methods 134: 9–21.

Dugué L, Merriam EP, Heeger DJ, and Carrasco M (2020) Differential impact of endogenous and exogenous attention on activity in human visual cortex. Sci Rep 10, 21274: 1-16.

Dugué L, Beck AA, Marque P, and VanRullen R (2019) Contribution of FEF to attentional periodicity during visual search: a TMS study. eNeuro 6: 1-10.

Dugué L, Merriam EP, Heeger DJ, and Carrasco M (2018) Specific visual subregions of TPJ mediate reorienting of spatial attention. Cerebral Cortex 28: 2375–2390.

Dugué L, and VanRullen R (2017) Transcranial magnetic stimulation reveals intrinsic perceptual and attentional rhythms. Frontiers in Neuroscience 11: 1-7.

Dugué L, Marque P, and VanRullen R (2015) Theta oscillations modulate attentional search performance periodically. Journal of Cognitive Neuroscience 27: 945–958.

Dugué L, Marque P, and VanRullen R (2011) The phase of ongoing oscillations mediates the causal relation between brain excitation and visual perception. J Neurosci 31: 11889–11893.

Fakche C, VanRullen R, Marque P, and Dugué L (2022) α Phase-amplitude tradeoffs predict visual perception. eNeuro: 1-16.

Fiebelkorn IC, Saalmann YB, and Kastner S (2013) Rhythmic sampling within and between objects despite sustained attention at a cued location. Current Biology 23: 2553–2558.

Gao X, Xu W, Wang Z, Takagaki K, Li B, and Wu JY (2012) Interactions between two propagating waves in rat visual cortex. Neuroscience 216: 57–69.

Girard P, Hupé J M, and Bullier J (2001) Feedforward and feedback connections between areas V1 and V2 of the monkey have similar rapid conduction velocities. J neurophysio 85(3): 1328-1331.

Graaf TA de, Gross J, Paterson G, Rusch T, Sack AT, and Thut G (2013) Alpha-band rhythms in visual task performance: Phase-locking by rhythmic sensory stimulation. PLOS ONE 8, e60035: 1-12.

Han F, Caporale N, and Dan Y (2008) Reverberation of recent visual experience in spontaneous cortical waves. Neuron 60: 321–327.

Heinrich SP (2010) Some thoughts on the interpretation of steady-state evoked potentials. Doc Ophthalmol 120: 205–214.

Henry MJ, Herrmann B, and Obleser J (2014) Entrained neural oscillations in multiple frequency bands comodulate behavior. PNAS 111: 14935–14940.

Henry MJ, and Obleser J (2012) Frequency modulation entrains slow neural oscillations and optimizes human listening behavior. PNAS 109: 20095–20100.

Horton J C, and Hoyt W F (1991) The representation of the visual field in human striate cortex: a revision of the classic Holmes map. Archives of ophthalmology 109(6): 816-824.

Huang Y, Chen L, and Luo H (2015) Behavioral oscillation in priming: competing perceptual predictions conveyed in alternating theta-band rhythms. J Neurosci 35: 2830–2837.

Huang X, Troy WC, Yang Q, Ma H, Laing CR, Schiff SJ, and Wu JY (2004) Spiral waves in disinhibited mammalian neocortex. J Neurosci 24: 9897–9902.

Jancke D, Chavane F, Naaman S, and Grinvald A (2004) Imaging cortical correlates of illusion in early visual cortex. Nature 428: 423–426.

Keitel C, Ruzzoli M, Dugué L, Busch N A, and Benwell C S (2022) Rhythms in cognition: The evidence revisited. European J Neurosci 55(11-12): 2991-3009.

Kienitz R, Schmid MC, and Dugué L (2022) Rhythmic sampling revisited: Experimental paradigms and neural mechanisms. European J Neurosci: 55(11-12), 3010-3024.

Kizuk SAD, and Mathewson KE (2017) Power and phase of alpha oscillations reveal an interaction between spatial and temporal visual attention. J Cog Neurosci 29: 480–494.

Landau AN, and Fries P (2012) Attention samples stimuli rhythmically. Current Biology 22: 1000–1004.

Lippert MT, Takagaki K, Xu W, Huang X, and Wu JY (2007) Methods for voltage-sensitive dye imaging of rat cortical activity with high signal-to-noise ratio. J Neurophysio 98: 502–512.

Liu-Shuang J, Norcia AM, and Rossion B (2014) An objective index of individual face discrimination in the right occipito-temporal cortex by means of fast periodic oddball stimulation. Neuropsychologia 52: 57–72.

Maris E, Womelsdorf T, Desimone R, and Fries P (2013) Rhythmic neuronal synchronization in visual cortex entails spatial phase relation diversity that is modulated by stimulation and attention. NeuroImage 74: 99–116.

Mathewson KE, Prudhomme C, Fabiani M, Beck DM, Lleras A, and Gratton G (2012) Making waves in the stream of consciousness: entraining oscillations in EEG alpha and fluctuations in visual awareness with rhythmic visual stimulation. J Cog Neurosci 24: 2321–2333.

Mathewson KE, Gratton G, Fabiani M, Beck DM, and Ro T (2009) To See or Not to See: Prestimulus α phase predicts visual awareness. J Neurosci 29: 2725–2732.

Merholz G, Grabot L, VanRullen R, and Dugué L (2022). Periodic attention operates faster during more complex visual search. Scientific Reports 12(1): 1-14.

Muller L, Chavane F, Reynolds J, and Sejnowski TJ (2018) Cortical travelling waves: mechanisms and computational principles. Nat Rev Neurosci 19: 255–268.

Muller L, Reynaud A, Chavane F, and Destexhe A (2014) The stimulus-evoked population response in visual cortex of awake monkey is a propagating wave. Nat Commun 5(1): 1-14.

Nauhaus I, Busse L, Ringach DL, and Carandini M (2012) Robustness of traveling waves in ongoing activity of visual cortex. J Neurosci 32: 3088–3094.

Nauhaus I, Busse L, Carandini M, and Ringach DL (2009) Stimulus contrast modulates functional connectivity in visual cortex. Nat Neurosci 12: 70–76.

Norcia AM, Appelbaum LG, Ales JM, Cottereau BR, and Rossion B (2015. The steady-state visual evoked potential in vision research: A review. Journal of Vision 15(6): 4-4

Nowak L G, and Bullier J (1996) Spread of stimulating current in the cortical grey matter of rat visual cortex studied on a new in vitro slice preparation. J Neurosci methods 67(2): 237-248.

Oever S ten, and Sack AT (2015) Oscillatory phase shapes syllable perception. PNAS 112: 15833–15837.

Prechtl JC, Bullock TH, and Kleinfeld D (2000) Direct evidence for local oscillatory current sources and intracortical phase gradients in turtle visual cortex. PNAS 97: 877–882.

Prechtl JC, Cohen LB, Pesaran B, Mitra PP, and Kleinfeld D (1997) Visual stimuli induce waves of electrical activity in turtle cortex. PNAS 94: 7621–7626.

Ray S, and Maunsell JHR (2011) Different origins of gamma rhythm and high-gamma activity in macaque visual cortex. PLOS Biology 9, e1000610: 1-9.

Reed AV (1973) Speed-accuracy trade-off in recognition memory. Science 181: 574–576.

Rekauzke S, Nortmann N, Staadt R, Hock HS, Schöner G, and Jancke D (2016) Temporal asymmetry in dark–bright processing initiates propagating activity across primary visual cortex. J Neurosci 36: 1902–1913.

Reynaud A, Masson GS, and Chavane F (2012) Dynamics of local input normalization result from balanced short- and long-range intracortical interactions in area V1. J Neurosci 32: 12558–12569.

Roland PE, Hanazawa A, Undeman C, Eriksson D, Tompa T, Nakamura H, Valentiniene S, and Ahmed B (2006) Cortical feedback depolarization waves: A mechanism of top-down influence on early visual areas. PNAS 103: 12586–12591.

Rossion B, Prieto EA, Boremanse A, Kuefner D, and Van Belle G (2012) A steady-state visual evoked potential approach to individual face perception: Effect of inversion, contrast-reversal and temporal dynamics. NeuroImage 63: 1585–1600.

Samaha J, Gosseries O, and Postle BR (2017) Distinct oscillatory frequencies underlie excitability of human occipital and parietal Cortex. J Neurosci 37: 2824–2833.

Samaha J, and Postle BR (2015) The speed of alpha-band oscillations predicts the temporal resolution of visual perception. Current Biology 25: 2985–2990.

Sanchez-Vives MV, and McCormick DA (2000) Cellular and network mechanisms of rhythmic recurrent activity in neocortex. Nat Neurosci 3: 1027–1034.

Sato TK, Nauhaus I, and Carandini M (2012) Traveling waves in visual cortex. Neuron 75: 218–229.

Shao Z, and Burkhalter A (1996) Different balance of excitation and inhibition in forward and feedback circuits of rat visual cortex. J Neurosci 16(22): 7353-7365.

Sharon D, Jancke D, Chavane F, Na'aman S, and Grinvald A (2007) Cortical response field dynamics in cat visual cortex. Cerebral Cortex 17: 2866–2877.

Sit YF, Chen Y, Geisler WS, Miikkulainen R, and Seidemann E (2009) Complex dynamics of V1 population responses explained by a simple gain-control model. Neuron 64: 943–956.

Slovin H, Arieli A, Hildesheim R, and Grinvald A (2002) Long-term voltage-sensitive dye imaging reveals cortical dynamics in behaving monkeys. J Neurophysio 88: 3421–3438.

Sokoliuk R, and VanRullen R (2016) Global and local oscillatory entrainment of visual behavior across retinotopic space. Sci Rep 6(1): 1-12.

Song WJ, Kawaguchi H, Totoki S, Inoue Y, Katura T, Maeda S, Inagaki S, Shirasawa H, and Nishimura M (2006) Cortical intrinsic circuits can support activity propagation through an isofrequency strip of the guinea pig primary auditory cortex. Cerebral Cortex 16: 718–729.

Spaak E, Lange FP de, and Jensen O (2014) Local entrainment of alpha oscillations by visual stimuli causes cyclic modulation of perception. J Neurosci 34: 3536–3544.

Sreekumar V, Wittig JH, Chapeton JI, Inati SK, and Zaghloul KA (2021) Low frequency traveling waves in the human cortex coordinate neural activity across spatial scales. bioRxiv: 1-48. https://doi.org/10.1101/2020.03.04.977173

Stefanics G, Hangya B, Hernádi I, Winkler I, Lakatos P, and Ulbert I (2010) Phase entrainment of human delta oscillations can mediate the effects of expectation on reaction speed. J Neurosci 30: 13578–13585.

Stroh A, Adelsberger H, Groh A, Rühlmann C, Fischer S, Schierloh A, Deisseroth K, and Konnerth A (2013) Making waves: Initiation and propagation of corticothalamic Ca2+ waves in vivo. Neuron 77: 1136–1150.

Takagaki K, Zhang C, Wu JY, and Lippert MT (2008) Crossmodal propagation of sensory-evoked and spontaneous activity in the rat neocortex. Neuroscience Letters 431: 191–196.

Takahashi K, Kim S, Coleman TP, Brown KA, Suminski AJ, Best MD, and Hatsopoulos NG (2015) Large-scale spatiotemporal spike patterning consistent with wave propagation in motor cortex. Nat Commun 6, 7169: 1-11.

Takahashi K, Saleh M, Penn R, and Hatsopoulos N (2011) Propagating waves in human motor cortex. Frontiers in Human Neuroscience 5: 1-8.

Townsend RG, Solomon SS, Chen SC, Pietersen ANJ, Martin PR, Solomon SG, and Gong P (2015) Emergence of complex wave patterns in primate cerebral cortex. J Neurosci 35: 4657–4662.

Valera FJ, Toro A, Roy John E, and Schwartz EL (1981) Perceptual framing and cortical alpha rhythm. Neuropsychologia 19: 675–686.

VanRullen, R (2016) Perceptual cycles. Trends in Cognitive Sciences 20: 723–735.

VanRullen R, and Dubois J (2011) The psychophysics of brain rhythms. Front Psychol: 1-10.

Watt J, Borhani R, and Katsaggelos AK (2020) Machine learning refined: Foundations, algorithms, and applications. Cambridge University Press.

Wickelgren WA (1977) Speed-accuracy tradeoff and information processing dynamics. Acta Psychologica 41: 67–85.

Xu W, Huang X, Takagaki K, and Wu J (2007) Compression and reflection of visually evoked cortical waves. Neuron 55: 119–129.

Yang Z, Heeger DJ, Blake R, and Seidemann E (2015) Long-range traveling waves of activity triggered by local dichoptic stimulation in V1 of behaving monkeys. J Neurophysio 113: 277–294.

Zanos TP, Mineault PJ, Nasiotis KT, Guitton D, and Pack CC (2015) A sensorimotor role for traveling waves in primate visual cortex. Neuron 85: 615–627.

Zhang H, and Jacobs J (2015) Traveling theta waves in the human hippocampus. J Neurosci 35: 12477–12487.

Zhang Q, Wen Y, Zhang D, She L, Wu J, Dan Y, and Poo M (2012) Priming with real motion biases visual cortical response to bistable apparent motion. PNAS 109: 20691–20696.